Available online at www.sciencedirect.com
ScienceDirect
Ceramics International 37 (2011) 265–271
CERAMICS INTERNATIONAL
www.elsevier.com/locate/ceramint

Impulse degradation behavior of Co–Cr–Al–Y-doped ZnO–Pr_6O_{11}-based varistors with sintering temperature

Choon-W. Nahm *

Semiconductor Ceramics Lab., Department of Electrical Engineering, Dongeui University, Busan 614-714, Republic of Korea

Received 10 June 2010; received in revised form 12 July 2010; accepted 27 August 2010
Available online 29 September 2010

Abstract

The degradation behavior against impulse-current stress of the Co–Cr–Al–Y-doped ZnO–Pr_6O_{11}-based varistors was investigated in accordance with sintering temperature. The clamp voltage ratio (K) for impulse current increased in accordance with increasing sintering temperature. The varistors sintered at 1300 °C exhibited the best voltage clamp characteristics, which the clamping voltage ratio was in the range of 1.49–1.57 at a low impulse-current region (5–10 A) and was in the range of 1.70–2.44 at a high impulse-current region (400–1200 A). The best electrical stability against multi-impulse stress for continuously 3 times 1200 A was obtained at 1350 °C in sintering temperature, where $\%\Delta E_{1\ mA/cm^2} = -5.0\%$, $\%\Delta\alpha = -13.9\%$, and $\%\Delta J_L = -21.9\%$.

Keywords: A. Sintering; E. Varistors; Electrical measurement; Impulse current stress; Clamp voltage ratio

1. Introduction

The sintered pellet of pure zinc oxide is polycrystalline ceramics and exhibits ohmic characteristics, which the current increases linearly in accordance with increasing applied voltage. On the contrary, the zinc oxide ceramics added with specific impurities exhibits varistor effect, which voltage–current (V–I) relation is nonlinear. The zinc oxide varistors are semiconducting ceramic devices formed by sintering zinc oxide with primary additives such as bismuth, praseodymium, vanadium, and subordinate additives such as cobalt, manganese, chrome, etc. They are voltage-dependent nonlinear resistors whose resistance decreases drastically when voltage is increased up to threshold voltage, called varistor voltage. In other words, at low voltage, varistor acts as a conventional high value resistor obeying ohms law [1]. They are play similar role to back-to-back Zener diode. However, zinc oxide varistors are multi-junction devices, which consisted of the microstructure of semiconducting ZnO grain-insulating intergranular layer-semiconducting ZnO grain, unlike Zener diode of single junction [2]. Thereby, they possess excellent surge withstanding capability. The zinc oxide varistors have been used extensively in the field of circuit overvoltage protection, with application ranging from a few volts in electronic circuits to millions of volts in electric power systems [3,4].

Recently, Zn–Pr-based varistor ceramics have been studied to further enhance the varistor properties and the stability against various stresses, compared with Zn–Bi-based varistor ceramics. Most investigations for Zn–Pr-based varistor ceramics have been reported on the microstructure and electrical properties in terms of additives and sintering process [5–17]. In particular, the effect of rare earth oxides and lanthanum oxides on electrical properties and its stability against DC accelerated aging stress was reported by Nahm, etc. [8–17].

In an application of varistors, the important factors that should be considered in the application are the nonlinearity, stability, and surge protection capability. The electronic equipments and the electrical power systems to be protected from various surges significantly demand a high stability of varistors in order to enhance reliability. Therefore, the electrical stability against various stresses is technologically very important in zinc oxide varistors, in particular impulse stress. However, a study on the effect of sintering process on the degradation behavior of the varistor properties against impulse stress with a high energy has been rarely reported [18–20]. In this work, the effect of sintering temperature on the degradation behavior against impulse-current

* Tel.: +82 51 890 1699; fax: +82 51 890 1664.
E-mail address: cwnahm@edu.ac.kr.

0272-8842/$36.00
doi:10.1016/j.ceramint.2010.09.017

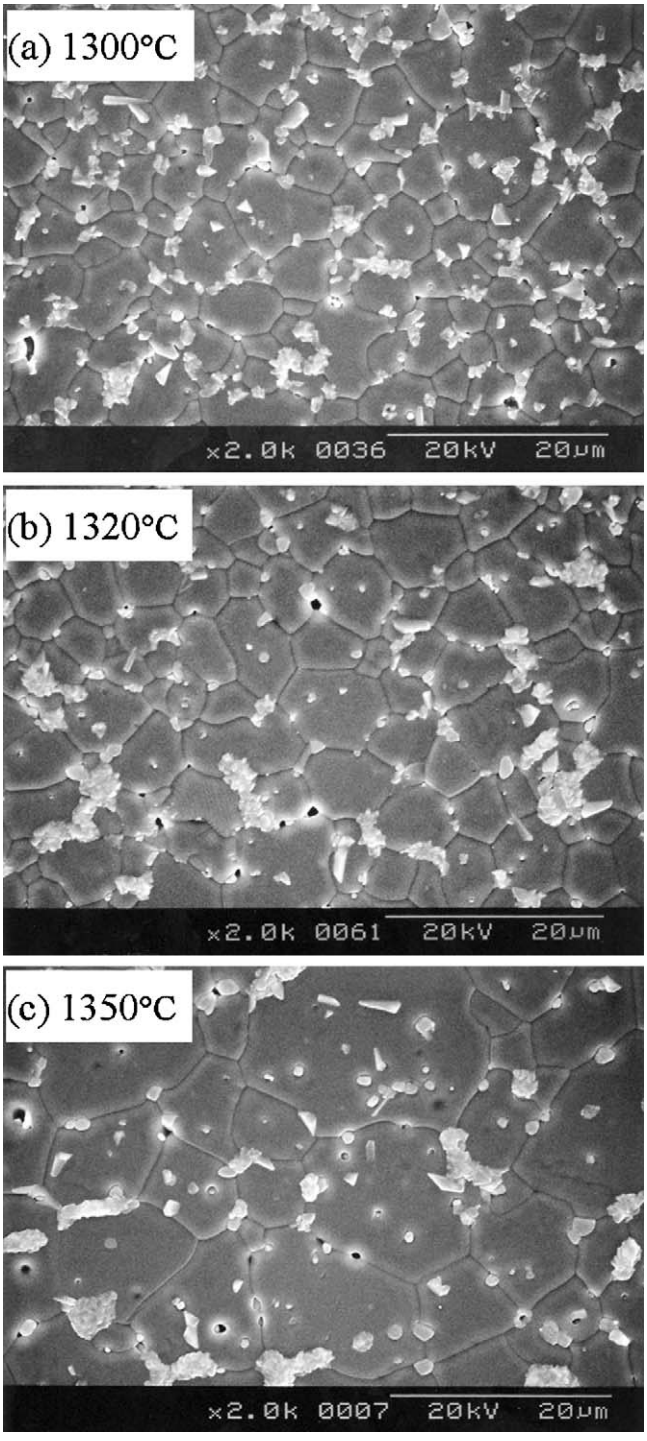

Fig. 1. SEM micrographs of the samples for different sintering temperatures.

stress in the Co–Cr–Al–Y-doped ZnO–Pr_6O_{11}-based varistors was addressed in accordance with sintering temperature and some new significant results were obtained.

2. Experimental procedure

2.1. Sample preparation

Reagent-grade raw materials were used in proportions of 97.495 mol% ZnO, 0.5 mol% Pr_6O_{11}, 1.0 mol% CoO, 0.5 mol% Cr_2O_3, 0.005 mol% Al_2O_3, and 0.5 mol% Y_2O_3. Raw materials were mixed by ball milling with zirconia balls and acetone in a polypropylene bottle for 24 h. The mixture was dried at 120 °C for 12 h and calcined in air at 750 °C for 2 h. The calcined mixture was pulverized using an agate mortar/pestle and after 2 wt% polyvinyl alcohol (PVA) binder addition, granulated by sieving through a 100-mesh screen to produce the starting powder. The powder was uniaxially pressed into discs of 10 mm in diameter and 2 mm in thickness at a pressure of 80 MPa. The discs were sintered at three fixed sintering temperatures (1300 °C, 1320 °C, 1350 °C) in air for 1 h and furnace-cooled to room temperature. The heating and cooling rates were 4 °C/min. The sintered samples were lapped and polished to 1.0 mm thickness. The final samples were about 8 mm in diameter and 1.0 mm in thickness. Silver paste was coated on both faces of samples and the silver electrodes were formed by heating it at 600 °C for 10 min. The electrodes were 5 mm in diameter. After soldering, the samples were packaged using a thermosetting resin.

2.2. Microstructure characterization

For microstructure characterization, both surfaces of the samples were lapped and ground with SiC paper and polished with 0.3 μm-Al powder to a mirror-like surface. The polished samples were thermally etched at 1100 °C for 30 min. The surface microstructure was examined by a scanning electron microscope (SEM, Hitachi S2400, Chiyoda-Ku, Tokyo, Japan). The average grain size (d) was determined by the lineal intercept method, given by $d = 1.56L/MN$, where L is the random line length on the micrograph, M is the magnification of the micrograph, and N is the number of the grain boundaries intercepted by the lines [21]. The density (ρ) of sintered ceramics was measured by the Archimedes method.

2.3. Electrical measurement

The electric field–current density (E–J) characteristics were measured using a V–I source (Keithley 237, Cleveland, OH, USA). The breakdown field ($E_{1\ mA/cm^2}$) was measured at

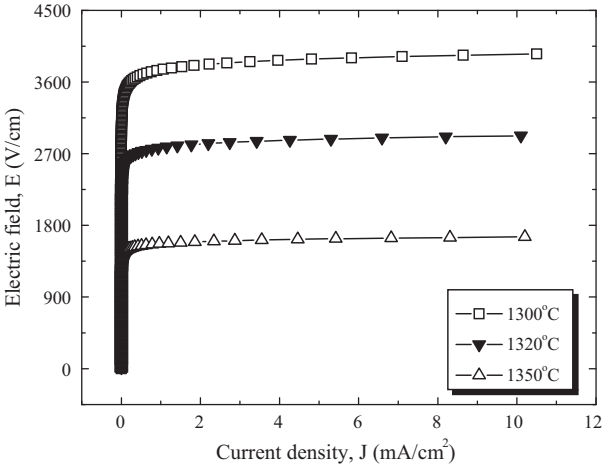

Fig. 2. E–J characteristic curves of the samples for different sintering temperatures.

Table 1
E–J characteristic parameters, clamping voltage (V_c), and clamp voltage ratio (K) of the samples for different sintering temperatures.

Sintering temp. (°C)	$E_{1\ mA/cm^2}$ (V/cm)	α	J_L (μA/cm^2)	$V_{1\ mA}$ (V/mm)	V_c (V)		$K = V_c/V_{1\ mA}$	
					I_p = 5 A	10 A	I_p = 5 A	10 A
1300	3754	46	5.9	389	580	610	1.49	1.57
1320	2776	44	5.4	288	470	480	1.63	1.67
1350	1572	43	3.2	163	267	274	1.64	1.68

1.0 mA/cm^2 and the leakage current density (J_L) was measured at 0.8 $E_{1\ mA/cm^2}$. In addition, the nonlinear coefficient (α) is defined by the empirical law, $J = C \cdot E^{\alpha}$, where J is the current density, E is the applied electric field, and C is a constant. α was determined in the current density range of 1.0 mA/cm^2 to 10 mA/cm^2, where $\alpha = 1/(\log E_2 - \log E_1)$, and E_1 and E_2 are the electric fields corresponding to 1.0 mA/cm^2 and 10 mA/cm^2, respectively.

2.4. Clamping voltage measurement

The clamping voltage (V_c) was measured at the 8 × 20 μs single impulse current (I_p) of 5 A, 10 A, 400 A, 900 A, and 1200 A using a surge generator (Tae-yang Eng. Kor) and oscilloscope (TeK 3020B, Beaverton, Oregon, USA). The clamp voltage ratio ($K = V_c/V_{1\ mA}$) is defined by ratio of clamping voltage to breakdown voltage. The breakdown voltage ($V_{1\ mA}$) was measured at a current of 1.0 mA DC.

2.5. Impulse degradation test

The single impulse degradation test was performed at the 8 × 20 (s single impulse-current (I_p) of 400 A, 900 A, 1200 A using a surge generator. The time interval between each impulse current stress cycle was 30 min. Furthermore, the multi-impulse degradation test was performed at a multi-impulse current stress of 1200 A for continuously 3 times with time interval of 2 min. After applying the impulse degradation stress, the *V–I* characteristics were measured at room temperature.

3. Results and discussion

Fig. 1 shows SEM micrographs of the samples for different sintering temperatures. There is no remarkable difference in the phases, which consisted of ZnO grain and intergranular in accordance with sintering temperature. XRD analysis (not shown) reveals the presence of Pr-rich and Y-rich intergranular layer as a minor secondary phase, in addition to a major phase of hexagonal ZnO [22,23]. The average grain size (d) increased in order of 5.6, 7.6 and 12.9 μm in accordance with increasing sintering temperature. The sintered density (ρ) for the samples was approximately 5.67 g/cm^3, corresponding to 98.1% of theoretical density (TD = 5.78 g/cm^3 in ZnO). Therefore, sintering temperature in the study for this composition did not significantly modify the densification process [22,23].

Fig. 2 shows the *E–J* characteristics of the samples for different sintering temperatures. The conduction characteristics of varistors are divided into a linear region with much higher impedance before breakdown field and a nonlinear region with much lower impedance after breakdown field. The *E–J* characteristic parameters calculated from Fig. 2 are summarized in Table 1. The breakdown field ($E_{1\ mA/cm^2}$) significantly decreased in a wide range from 3754 to 1572 V/cm in accordance with increasing sintering temperature. This is attributed to the decrease in the number of grain boundaries caused by the increase in the ZnO grain size. On the other hand, the nonlinear coefficient (α) slightly decreased by a narrow margin from 46 to 43 in accordance with increasing sintering temperature. The decrease in α value is attributed to the lowering of the Schottky barrier because of the variation of the electronic state at the grain boundaries [22,23]. On the whole, the α value was close to 45 in the range of the specified sintering temperature. This shows that the nonlinear properties are not greatly affected by sintering temperature for the range of sintering temperatures tested in this study, unlike the breakdown field. Therefore, this system has the advantage of applications because it has a nearly constant nonlinear coefficient over a wide range of sintering temperatures. The leakage current density (J_L) increased from 5.9 μA/cm^2 to 3.2 μA/cm^2 in accordance with increasing sintering temperature.

Fig. 3 shows the clamping voltage (V_c) characteristics corresponding to the impulse-current for different sintering temperatures. The V_c is defined by the drop voltage between electrodes of the sample when the specified impulse-current flows through the sample. The higher impulse-current leads to the higher V_c because the resistance in the nonlinear region exists still as a low value. It can be seen that the higher breakdown voltage leads to the higher clamping voltage. The detailed clamping voltage (V_c) and clamp ratio (K) corresponding to impulse-current are summarized in Table 1. The low K value means that the varistor well clamps an impulse-current to operating voltage. With increasing sintering temperature, the K value increased from 1.46 to 1.64 at an impulse-current of 5 A and from 1.57 to 1.68 at an impulse-current of 10 A. All the samples exhibited good clamp characteristics, as recording clamping ratio far less than 2 in K. Table 2 shows the V_c and K value at a higher impulse-current region (400–1200 A). Also the K value increased in the same way as low impulse-current region (5–10 A) in accordance with increasing sintering temperature. Based on α and K value in Tables 1 and 2, it can be seen that higher α value lead to low K value. In order to obtain low K value, the α measured in the range of 1.0 mA/cm^2 and 10 mA/cm^2 have to be maintained it up to high current region. On the whole, it can be seen that the nonlinearity of all the samples maintains up to 1200 A certainly. In the light of

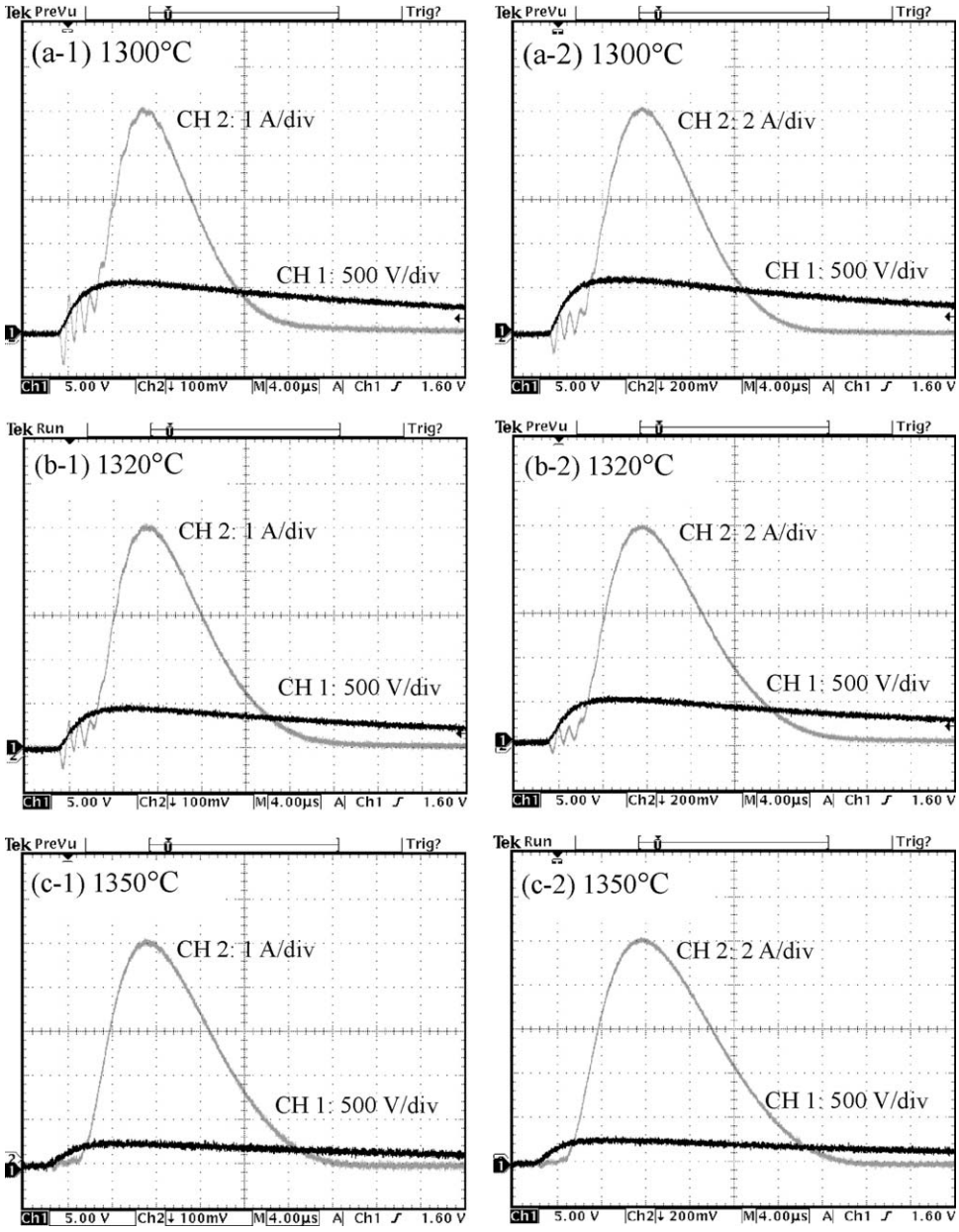

Fig. 3. Clamping voltage waveforms for impulse-current of the samples for different sintering temperatures.

data shown in Tables 1 and 2, it can be seen that the samples sintered at 1300 °C show the best clamping characteristics for an impulse-current.

Fig. 4 compares the variation of *E–J* characteristics after applying the impulse impulse stress (400, 900, 1200 A) with initial for different sintering temperatures. Impulse-current stress of 900 A and 1200 A is very severe, compared with a surge current applied to commercial varistors. The variation of *E–J* characteristics after applying the impulse stress decreased in accordance with increasing sintering temperature. It can be seen that the *E–J* characteristic curve shifted toward a low field region (downward in Fig. 4) in breakdown region after

Table 2
Clamping voltage (V_c), and clamp voltage ratio (K) of the samples at a higher impulse-current for different sintering temperatures.

Sintering temp. (°C)	$V_{1\ mA}$ (V/mm)	V_c (V)			$K = V_c/V_{1\ mA}$		
		I_p = 400 A	900 A	1200 A	I_p = 400 A	900 A	1200 A
1300	389	662	856	950	1.70	2.20	2.44
1320	288	506	640	714	1.76	2.22	2.48
1350	163	293	372	410	1.80	2.28	2.51

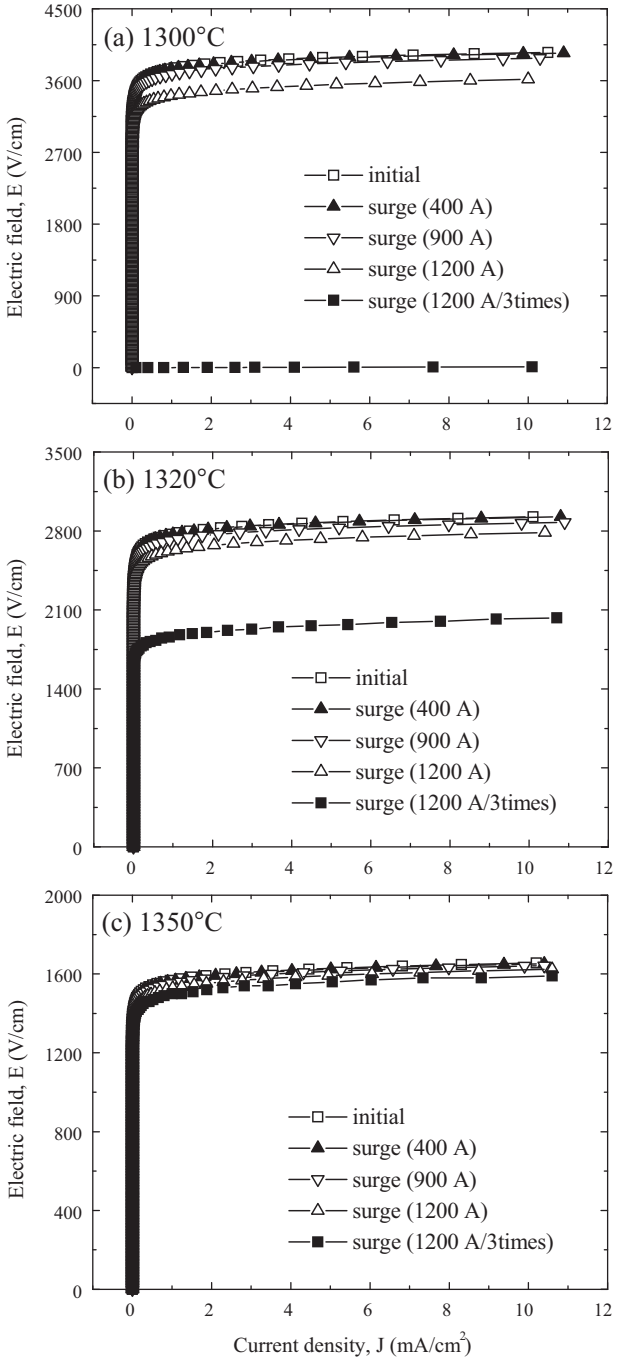

Fig. 4. *E–J* characteristic curves after applying the impulse aging stress of the samples for different sintering temperatures.

applying the impulse stress. This is entirely different with *E–J* characteristic behavior, which shifted toward a high current region (rightward) in prebreakdown region after applying the DC accelerated aging stress [15]. It can be seen that sintering temperature has a great effect on electrical characteristics from the variation of characteristic curves with increasing impulse-current. Seemingly, as the single impulse strength increased in the range of 400–1200 A, the *E–J* characteristic variation with sintering temperature is not so large. However, when the multi-impulse stress of 1200 A was applied continuously 3 times to the samples, the samples sintered at 1300 °C were destroyed

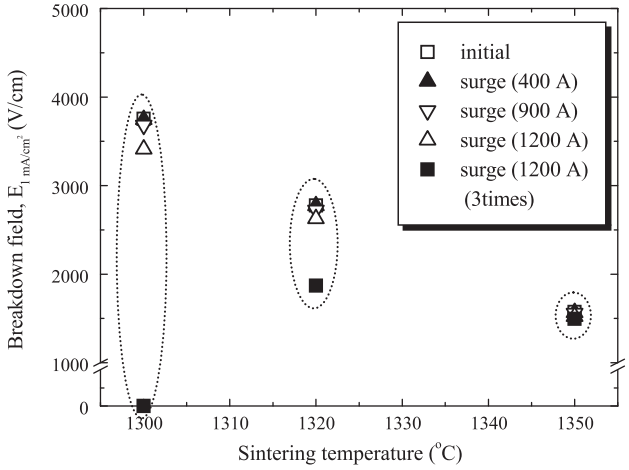

Fig. 5. Variation of breakdown field after applying the impulse aging stress of the samples for different sintering temperatures.

and it exhibited completely ohmic properties with very low resistance. The samples sintered at 1300 °C exhibited a large variation, compared with single impulse stress of 1200 A. However, the samples sintered at 1350 °C exhibited very stable *E–J* characteristics.

Fig. 5 compares the variation of breakdown field ($\%\Delta E_{1\ mA/cm^2}$) after applying the impulse stress with initial for different sintering temperatures. The $\%\Delta E_{1\ mA/cm^2}$ after applying the single impulse stress of 1200 A was −9.2% for the samples sintered at 1300 °C, −5.4% for the samples sintered at 1320 °C, and −3.2% for the samples sintered at 1350 °C. All the samples show good stable $E_{1\ mA/cm^2}$ characteristics against the single impulse stress, as recording the variation rate less than 10%. Furthermore, the $\%\Delta E_{1\ mA/cm^2}$ after applying the multi-impulse stress of 1200 A was −32.6% for the samples sintered at 1320 °C and −5.0% for the samples sintered at 1350 °C, As a result, the samples sintered at 1350 °C exhibited the best stable breakdown field against impulse stress.

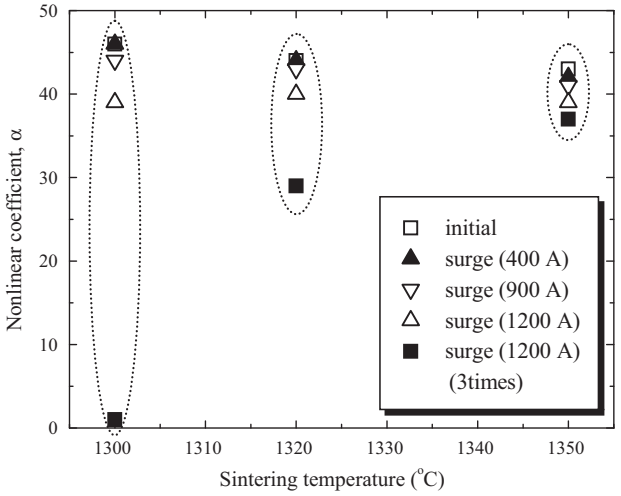

Fig. 6. Variation of nonlinear coefficient after applying the impulse aging stress of the samples for different sintering temperatures.

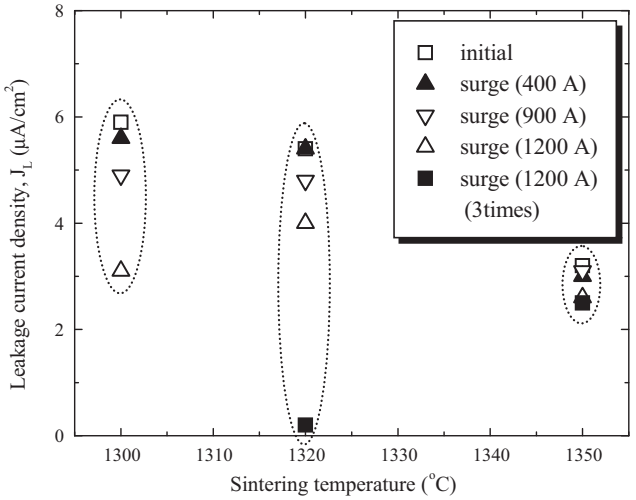

Fig. 7. Variation of leakage current density after applying the impulse aging stress of the samples for different sintering temperatures.

Fig. 6 compares the variation of nonlinear coefficient ($\%\Delta\alpha$) after applying the impulse stress with initial for different sintering temperatures. The $\%\Delta\alpha$ after applying the single impulse stress of 1200 A was −15.2% for the samples sintered 1300 °C, −9.1% for the samples sintered at 1320 °C, and −9.3% for the samples sintered at 1350 °C. Furthermore, The $\%\Delta\alpha$ after applying the multi-impulse stress of 1200 A was −30.1% for the samples sintered at 1320 °C and −13.9% for the samples sintered at 1350 °C. As a result, the samples sintered at 1350 °C exhibited the best stable nonlinear properties against impulse stress.

Fig. 7 compares the variation of leakage current density ($\%\Delta J_L$) after applying the impulse stress with initial for different sintering temperatures. The $\%\Delta J_L$ after applying the single impulse stress of 1200 A was −47.4% for the samples sintered 1300 °C, −25.9% for the samples sintered at 1320 °C, and −18.7% for the samples sintered at 1350 °C. Furthermore, the $\%\Delta J_L$ after applying the multi-impulse stress of 1200 A was −96.3% for the samples sintered at 1320 °C and −21.9% for the samples sintered at 1350 °C. The samples sintered at 1350 °C exhibited the ΔJ_L less than roughly 20% with impulse stress, whereas the samples sintered at 1320 °C exhibited the decrease of very low J_L after applying the multi-impulse stress of 1200 A. On the whole, it is assumed that the decrease of leakage current with impulse stress for respective sample is attributed to decrease of recombination current into double Schottky barrier.

As just addressed above, it can be seen that the sintering temperature has a significant effect on the stability against impulse degradation stress. Increasing sintering temperature led to more stable *E–J* characteristics against impulse stress. The samples sintered at 1350 °C exhibited the best stable *E–J* characteristics against impulse stress, unlike voltage clamp characteristics in accordance with increasing sintering temperature. In DC-accelerated aging stress test of 0.95 $E_{1\ mA/cm^2}$/150 °C/24 h, it was found that the samples sintered at 1300 °C exhibited the thermal run-away for and the samples sintered at 1350 °C exhibited a large characteristic variation without thermal runaway, compared with the samples sintered at 1320 °C [19]. As a result, the samples sintered at 1320 °C exhibited the best characteristics in terms of nonlinear properties and DC-accelerated aging stress characteristics. However, in the light of totally varistor application, sintering temperature in this study is optimized at 1350 °C.

4. Conclusions

The effect of sintering temperature on the degradation behavior against impulse-current stress in the Co–Cr–Al–Y-doped ZnO–Pr_6O_{11}-based varistors was investigated. The increase of sintering temperature increased the clamp voltage ratio (*K*) and exhibited good clamping characteristics. The varistor sintered at 1300 °C exhibited the lowest *K* value, which is 1.49 at an impulse-current of 5 A and 1.57 at an impulse-current of 10 A. The best electrical stability against multi-impulse stress of 1200 A was obtained at 1350 °C, where $\%\Delta E_{1\ mA/cm^2} = -5.0\%$, $\%\Delta\alpha = -13.9\%$, and $\%\Delta J_L = -21.9\%$. Conclusively, it is assumed that sintering temperature will be optimized at 1350 °C considering several factors, such as a nonlinearity, DC accelerated aging characteristics, impulse degradation characteristics, and so on.

References

[1] C.-W. Nahm, Effect of sintering time on stability of nonlinear properties in Dy_2O_3-doped ZnO–Pr_6O_{11}-based varistors, Mater. Lett. 58 (2004) 3769–3773.
[2] C.-W. Nahm, The electrical properties and d.c. degradation characteristics of Dy_2O_3 doped Pr_6O_{11}-based ZnO varistors, J. Eur. Ceram. Soc. 21 (2001) 545–553.
[3] L.M. Levinson, H.R. Philipp, Zinc oxide varistor—a review, Am. Ceram. Soc. Bull. 65 (1986) 639–646.
[4] T.K. Gupta, Application of zinc oxide varistor, J. Am. Ceram. Soc. 73 (1990) 1817–1840.
[5] A.B. Alles, V.L. Burdick, The effect of liquid-phase sintering on the properties of Pr_6O_{11}-based ZnO varistors, J. Appl. Phys. 70 (1991) 6883–6890.
[6] A.B. Alles, R. Puskas, G. Callahan, V.L. Burdick, Compositional effect on the liquid-phase sintering of praseodymium oxides-based ZnO varistors, J. Am. Ceram. Soc. 76 (1993) 2098–2102.
[7] Y.-S. Lee, K.-S. Liao, T.-Y. Tseng, Microstructure and crystal phases of praseodymium in zinc oxides varistor ceramics, J. Am. Ceram. Soc. 79 (1996) 2379–2384.
[8] C.-W. Nahm, The nonlinear properties and stability of ZnO–Pr_6O_{11}–CoO–Cr_2O_3–Er_2O_3 ceramic varistors, Mater. Lett. 47 (2001) 182–187.
[9] C.-W. Nahm, J.-S. Ryu, Effect of sintering temperature on electrical properties and stability of Pr_6O_{11}-based ZnO varistors, J. Mater. Sci.: Mater. Electron. 13 (2002) 111–120.
[10] C.-W. Nahm, B.-S. Shin, M.-H. Min, Microstructure and electrical properties of Y_2O_3-doped ZnO–Pr_6O_{11}-based varistor ceramics, Mater. Chem. Phys. 82 (2003) 157–164.
[11] C.-W. Nahm, B.-C. Shin, Effect of sintering time on electrical properties and stability against DC accelerated aging of Y_2O_3-doped ZnO–Pr_6O_{11}-based varistor ceramics, Ceram. Int. 30 (2004) 9–15.
[12] C.-W. Nahm, Microstructure and electrical properties of Dy_2O_3-based ZnO–Pr_6O_{11}-based varistor ceramics, Mater. Lett. 58 (2004) 2252–2255.
[13] C.-W. Nahm, B.-C. Shin, Effect of sintering time on electrical characteristics and DC accelerated aging behaviors of Zn–Pr–Co–Cr–Dy oxide-based varistors, J. Mater. Sci.: Mater. Electron. 16 (2005) 725–732.

[14] C.-W. Nahm, Influence of La_2O_3 additives on microstructure and electrical properties of ZnO–Pr_6O_{11}–CoO–Cr_2O_3-based varistors, Mater. Lett. 59 (2005) 2097–2100.
[15] C.-W. Nahm, Effect of sintering temperature on nonlinear electrical properties and stability against DC accelerated aging stress of (CoO, Cr_2O_3, La_2O_3)-doped ZnO–Pr_6O_{11}-based varistors, Mater. Lett. 60 (2006) 3311–3314.
[16] C.-W. Nahm, Microstructure and non-ohmic properties of ZPCCT-based ceramics, J. Mater. Sci. 41 (2006) 8382–8385.
[17] C.-W. Nahm, Electrical properties and stability of Tb-doped ZnO-based nonlinear resistors, Solid State Commun. 141 (2007) 685–690.
[18] C.-W. Nahm, Effect of cooling rate on electrical properties, impulse surge and dc-accelerated aging behavior of ZPCCD-based varistors, J. Mater. Sci.: Mater. Electron. 20 (2009) 418–424.
[19] C.-W. Nahm, Electrical behavior against current impulse in ZnO–Pr_6O_{11}-based varistor ceramics with terbium addition, Ceram. Int. 36 (2010) 1495–14501.
[20] C.-W. Nahm, Al doping effect on electrical and dielectric aging behavior against impulse surge in ZPCCYA-based varistors, Mater. Sci. Eng. B 170 (2010) 123–128.
[21] J.C. Wurst, J.A. Nelson, Lineal intercept technique for measuring grain size in two-phase polycrystalline ceramics, J. Am. Ceram. Soc. 55 (1972) 109–111.
[22] C.-W. Nahm, The effect of sintering temperature on varistor properties of (Pr, Co, Cr, Y, Al)-doped ZnO ceramics, Mater. Lett. 62 (2008) 4440–4442.
[23] C.-W. Nahm, Sintering temperature dependence of varistor properties and aging behavior in ZnO–Pr_6O11–CoO–Cr_2O_3-Al_2O_3-Y_2O_3 ceramics, Am. Ceram. Soc. 93 (2010) 2297–2304.